Three-dimensional *T*-stresses for three-point-bend specimens with large thickness variation

Kai Lu[1*], Toshiyuki Meshii[2]

[1] Graduate School of Engineering, University of Fukui, 3-9-1 Bunkyo, Fukui, Fukui, Japan
[2] Faculty of Engineering, University of Fukui, 3-9-1 Bunkyo, Fukui, Fukui, Japan
* Corresponding author: kai_lu@u-fukui.ac.jp FAX : +81-776-27-9764

Abstract

Three-point-bend (3PB) test specimens are useful for the systematic investigation of the influence of statistical and constraint loss size effects on the cleavage fracture toughness of a material in the ductile-to-brittle transition temperature range. Because the in- and out-of-plane elastic *T*-stresses (T_{11} and T_{33}) are a measure of the crack-tip constraint and even the in-plane T_{11} exhibits three-dimensional (3D) effects, the 3D *T*-stresses solutions were obtained by running finite element analyses (FEA) for 3PB specimens with wide ranges of the crack depth-to-width ratio (a/W = 0.2 to 0.8) and the specimen thickness-to-width ratio (B/W = 0.1 to 40). The results show that the 3D T_{11} at the specimen mid-plane tended to deviate from the 2D T_{11} as B/W increased, with the deviation saturating for $B/W \geq 2$. The mid-plane T_{33} increased with B/W and was close to the plane strain value νT_{11} for $B/W \geq 2$.

Keywords: Elastic *T*-stress, Three-point-bend specimen, Finite element analysis, Fracture toughness, Constraint effect

Nomenclature

B	Specimen thickness
E	Young's modulus
F	Unit magnitude (see Eq. (2))
I	Interaction integral
K_I	Local mode I stress intensity factor (SIF)
K_0	2D SIF for elastic analysis
R_s	Crack tube radius
S	Support span for 3PB specimen
T_{11}, T_{33}	*T*-stresses

W	Specimen width
a	Crack length
r, θ	In-plane polar coordinates
x_j	Crack-tip local coordinates (j = 1, 2, 3)
Δ	Singular element size
β_{11}, β_{33}	Normalized T-stresses
ε_{33}	Out-of-plane strain
ν	Poisson's ratio
σ_{ij}	Stress components (i, j = 1, 2, 3)

1. Introduction

Three-point-bend (3PB) test specimens are useful for the systematic investigation of the statistical and constraint loss size effects on the cleavage fracture toughness of a material in the ductile-to-brittle transition temperature range [1, 2]. Because the in-plane and out-of-plane T-stresses (T_{11} and T_{33}) are a measure of the crack-tip constraint and even the in-plane T_{11} exhibits three-dimensional (3D) effects [2-4], the 3D T-stresses solutions were obtained by running finite element analyses (FEA) for 3PB specimens with wide ranges of the crack depth-to-width ratio (a/W = 0.2 to 0.8) and the specimen thickness-to-width ratio (B/W = 0.1 to 40). The 2D T_{11} solutions have been provided for 3PB specimen in many numerical studies [5-10].

The results show that the 3D T_{11} at the specimen mid-plane tended to deviate from the 2D T_{11} as B/W increased, with the deviation saturating for $B/W \geq 2$. The mid-plane 3D T_{11} for B/W = 0.1 to 40 was high as 54% when a/W = 0.2, suggesting that 3D effects should be properly considered for cases of short crack length, especially when T_{11} is negative. The mid-plane T_{33} increased with B/W and was close to the plane strain value of T_{11} for $B/W \geq 2$.

2. *T*-stress

In an isotropic linear elastic body containing a crack subjected to symmetric (mode I) loading, the Williams series expansion [11] of the 3D stress components near the crack tip field can be written as [3]

$$\begin{Bmatrix}\sigma_{11}\\ \sigma_{22}\\ \sigma_{33}\\ \tau_{12}\\ \tau_{23}\\ \tau_{31}\end{Bmatrix}=\frac{K_I}{\sqrt{2\pi r}}\begin{Bmatrix}\cos\frac{\theta}{2}\left(1-\sin\frac{\theta}{2}\sin\frac{3\theta}{2}\right)\\ \cos\frac{\theta}{2}\left(1+\sin\frac{\theta}{2}\sin\frac{3\theta}{2}\right)\\ 2\nu\cos\frac{\theta}{2}\\ \sin\frac{\theta}{2}\cos\frac{\theta}{2}\cos\frac{3\theta}{2}\\ 0\\ 0\end{Bmatrix}+\begin{Bmatrix}T_{11}\\ 0\\ T_{33}\\ 0\\ 0\\ 0\end{Bmatrix} \quad (1)$$

where r and θ are the in-plane polar coordinates of the plane normal to the crack front shown in Fig. 1, K_I is the local mode I stress intensity factor (SIF) and ν is Poisson's ratio. Here, x_1 is the direction formed by the intersection of the plane normal to the crack front and the plane tangential to the crack plane. T_{11} and T_{33} are the amplitudes of the second-order terms in the three-dimensional series expansions of the crack front stress field in the x_1 and x_3 directions, respectively.

Different methods have been applied to compute the elastic *T*-stress for test specimens, as summarized by Sherry et al. [10]. In this study, an efficient finite element method developed by Nakamura and Parks [11] based on an interaction integral was used to determine the elastic *T*-stresses.

The crack tip T_{11}-stress on the crack front is related to the interaction integral by

$$T_{11}=\frac{E}{1-\nu^2}\left\{\frac{I}{F}+\nu\varepsilon_{33}\right\} \quad (2)$$

where E is Young's modulus, ν is Poisson's ratio and ε_3 identifies the out-of-plane strain at the crack tip in the direction tangential to the crack front. I represents the interaction integral, and F indicates the unit magnitude (F = 1).

Once the T_{11}-stress is obtained, the T_{33}-stress can be obtained using the following relationship:

$$T_{33}=E\varepsilon_{33}+\nu T_{11} \quad (3)$$

More details of this method can be found in Nakamura and Parks [11] and Qu and Wang [12].

3. Finite Element Analysis (FEA)

3.1 Description of the finite element model

In the present study, 3D elastic FEA was conducted to calculate the elastic *T*-stresses (T_{11} and T_{33}) for a 3PB test specimen with a straight crack. Fig. 2 shows a sketch of the loads and geometry. In this figure, a, B, W and S are the crack length and the specimen thickness, width and support span,

respectively. For all current calculations, the specimen width was set as W = 25 mm, with a support span of $S = 4W$.

To systematically quantify the out-of-plane crack-tip constraint effect of the 3PB specimen, the thickness-to-width ratios B/W = 0.1, 0.25, 0.5, 1, 1.5, 2 and 40 were considered to cover the B/W range studied experimentally by Rathbun et al. [1]. For each B/W, the crack depth-to-width ratios a/W = 0.2, 0.3, 0.4, 0.45, 0.5, 0.55, 0.6, 0.7 and 0.8 were considered to investigate the in-plane constraint.

The material is assumed to be linearly elastic (isotropic and homogeneous). Young's modulus E = 206 GPa and Poisson's ratio ν= 0.3 were set based on ferritic steel, which is the most widely used material in engineering. 3D finite elements were used to build a one-quarter symmetric model of the 3PB specimen, as shown in Fig. 3(a). The finite element model used 20-noded isoparametric 3D solid elements with reduced (2×2×2) Gauss integration. Sixteen singular elements were used around the crack tip for all cases in this study. Twenty equivalent rows of meshes were spaced inside the crack tube with radius R_s = 0.4 mm (Fig. 3(b)). In the present FEA models, 365740 to 393194 nodes with 86912 to 93840 elements were used, and the details for the generated mesh are summarized in the Appendix.

WARP3D [13] was used as the FEA solver. The load set for the elastic FEA corresponded to the 2D SIF K_0 = 1 MPa m$^{1/2}$ calculated from the following equation from the ASTM standard [14].

$$K = \frac{PS}{BW^{3/2}} f(a/W) \qquad (4)$$

where f is a function of a/W and is defined in the standard.

3.2 T-stresses for 3PB specimens

T_{11} was evaluated as the average of the values of T_{11} obtained from domain 2 to domain 20. Good independence of the T value on the choice of domain was obtained, as the differences in the T-stress results from domain 2 to domain 20 were within 1% of one another, except for the values in the vicinity of the free surface. The obtained mid-plane T_{11} and T_{33} stresses are summarized in Tables 1 and 2, respectively, in the normalized form of $\beta_{kk} = T_{kk}(\pi a)^{1/2}/K_0$ (k = 1 or 3). The T-stresses at the specimen mid-plane received special attention because fracture initiation occurs at this location (e.g., [1, 2]).

First, the obtained mid-plane β_{11} values were compared with the 2D β_{11} solutions obtained by different authors [5-9] as a validity check. Sherry et al. reported that these 2D solutions varied significantly [10] and compiled them as a polynomial function of a/W. However, in this work, Kfouri's plane-strain solutions [6] were chosen for comparison with our 3D β_{11} solutions based on the expectation that the 3D β_{11} will approach the plane-strain values, as shown in Fig. 4(a). The mid-plane β_{11} exhibited 3D effects and monotonously decreased with increasing B/W but saturated to

values very close to the plane-strain solutions, as shown in Fig. 4(b). This tendency was similar to that observed by Nakamura and Parks for a single edge-cracked plate under pure bending [3].

Another finding was that β_{11} was a monotonously increasing function of a/W, regardless of B/W. The results showed that negative β_{11}, and thus loss of the in-plane crack-tip constraint, was anticipated for cases of $a/W \leq 0.3$.

Fig. 5 shows the mid-plane β_{33} solutions for various thicknesses and crack depths. In Fig. 5(a), it is observed that β_{33} is a monotonously increasing function of B/W, as expected. The bounding value of β_{33} for each a/W was close to the plane strain value of β_{11}, and a relative thickness of $B/W = 40$ was sufficient for β_{33} to saturate to the bounding value, as shown in Fig. 5(b).

β_{33} for the ASTM standard 3PB specimen [14], for which $B/W = 0.5$ and $0.45 \leq a/W \leq 0.55$, was negative. This finding seemed to support the fact that J_c was not bounded in the case of increasing B/W for 3PB specimens [1].

Interestingly, in Fig. 5(b), β_{33} was not always a monotonously increasing function of a/W, as observed for the thin specimens of $B/W = 0.1$, 0.25 and 0.5. For example, β_{33} for $B/W = 0.1$ was a monotonously decreasing function of a/W and thus might lead to the incorrect conclusion that deep cracks lose the out-of-plane crack-tip constraint. However, by normalizing T_{33} in terms of $T_{33}(\pi W)^{1/2}/K_0$ (W was constant for all cases in this study) as shown in Fig. 6, it is clearly seen that T_{33} increased monotonously as a/W increased for all B/Ws, which means that the out-of-plane crack-tip constraint level was strengthened due to the increase in crack depth, although the increase rate was smaller than $a^{1/2}$.

4. Discussion

In addition to the mid-plane T-stresses, the variations of the β_{11} and β_{33} solutions in the thickness direction were also plotted for various thicknesses for $a/W = 0.5$ in Fig. 7 and 8, respectively. Note that the mid-side node values were omitted in this figure. As observed in the left part of Fig. 7, the in-plane β_{11} distributions changed little overall compared with the mid-plane value in the range of $x_3/(B/2) = 0$ to 0.8. Specifically, these differences were in the range of 4.1 to 15.3%. The differences were less than 5% if $x_3/(B/2)$ was in the range of 0 to 0.5, regardless of B/W.

On the other hand, the out-of-plane β_{33} distributions in Fig. 8 showed a visible decrease in the thickness direction, considering that the ordinate of this figure ranges from -14 to 2. However, the rate of decrease became small as B/W increased, as is clear for the case of $B/W = 40$. Note that both T_{11} and T_{33} diverged significantly in the vicinity of the free surface ($x_3/(B/2) = 0.8$ to 1.0) because ε_{33} tends to be singular near the free surface and is not well calculated using FEA [3, 4]. Thus, the T-stresses near the free surface calculated by the present FEA method are known to be unreliable [12] and require further study.

5. Summary

In the present study, the T-stress solutions for 3PB specimens with a wide range of the crack depth-to-width ratio (a/W = 0.2 to 0.8) and the specimen thickness-to-width ratio (B/W = 0.1 to 40) were calculated using 3D elastic FEA. The results showed that 3D T_{11} at the specimen mid-plane tended to deviate from the 2D T_{11} as B/W increased, with the deviation saturating for $B/W \geq 2$. The mid-plane 3D T_{11} between cases of B/W = 0.1 and 40 was large as 54% for a/W = 0.2 and suggested that the 3D effects should be properly considered for cases of short crack length, especially when T_{11} is negative. The mid-plane T_{33} increased with B/W and was close to the plane strain value of T_{11} for $B/W \geq 2$.

Acknowledgments

This work was supported in part by JSPS KAKENHI Grant Number 24561038. Their support is greatly appreciated.

Appendix

List of figures

References

[1] Rathbun HJ, Odette GR, Yamamoto T, Lucas GE. Influence of statistical and constraint loss size effects on cleavage fracture toughness in the transition-A single variable experiment and database. Engineering Fracture Mechanics. 2006;73:134-58.

[2] Meshii T, Lu K, Takamura R. A failure criterion to explain the test specimen thickness effect on fracture toughness in the transition temperature region. Engineering Fracture Mechanics. 2013;104: 184-197.

[3] Nakamura T, Parks DM. Determinationof elastic *T*-stress along three-dimensional crack fronts using an interaction integral. International Journal of Solids and Structures. 1992;29(13):1597-1611.

[4] Fernández-Canteli A, Giner E, Fernández-Sáez J, Fernández- Zúñiga. A unified analysis of the in-plane and out-of-plane constraints in 3-D linear elastic fracture toughness, Proceedings of the 19th European Conference on Fracture. Kazan, Russia. 2012; p.1-8.

[5] Leevers PS, Radon JC. Inherent stress biaxiality in various fracture specimen geometries. International Journal of Fracture. 1982;19:311-325.

[6] Kfouri AP. Some evaluations of the elastic *T*-term using Eshelby's method. International Journal of Fracture. 1986;30(4):301-315.

[7] Cardew GE, Goldthorpe MR, Howard IC, Kfouri AP. On the Elastic *T*-term. In: Bibly BA, Miller KJ, Willis JR, editors. Fundamentals of Deformation and Fracture. Cambridge: Cambridge University Press; 1984. p. 465-476.

[8] Fett T. *T*-stresses in rectangular plates and circular disks. Engineering Fracture Mechanics. 1998;60(5-6):631-652.

[9] Yang B, Ravi-Chandar K. Evaluation of elastic *T*-stress by the stress difference method. Engineering Fracture Mechanics. 1999;64(5):589-605.

[10] Sherry AH, Moran B, Nakamura T. Compendium of *T*-stress solutions for two and three dimensional cracked geometries. Fatigue and Fracture of Engineering Materials and Structures. 1995;18:141-155.

[11] Williams ML. On the stress distribution at the base of a stationary crack. Journal of Applied Mechanics. 1957;24:111-114.

[12] Qu J, Wang X. Solutions of *T*-stresses for quarter-elliptical corner cracks in finite thickness plates subject to tension and bending. International Journal of Pressure Vessels and Piping. 2006;83(8):593-606.

[13] Gullerud A, Koppenhoefer K, Roy Y, RoyChowdhury S, Walters M, Bichon B, et al. WARP3D Release 15 Manual. Civil Engineering, Report No UIUCENG-95-2012, University of Illinois at Urbana-Champaign. 2004.

[14] ASTM. E1921-10 Standard test method for determination of reference temperature, T_0, for ferritic steels in the transition range. Annual Book of ASTM Standards. Philadelphia PA: American Society for Testing and Materials; 2010.

Table 1. Normalized T_{11} solutions (β_1) at the specimen mid-plane for 3PB specimens (ν= 0.3).

a/W									
B/W	**0.2**	**0.3**	**0.4**	**0.45**	**0.5**	**0.55**	**0.6**	**0.7**	**0.8**
0.1	**-0.158**	**-0.022**	**0.115**	**0.185**	**0.258**	**0.334**	**0.415**	**0.605**	**0.876**
0.25	**-0.182**	**-0.055**	**0.079**	**0.149**	**0.221**	**0.297**	**0.379**	**0.576**	**0.866**
0.5	**-0.188**	**-0.059**	**0.073**	**0.143**	**0.216**	**0.294**	**0.379**	**0.574**	**0.820**
1	**-0.220**	**-0.078**	**0.063**	**0.133**	**0.204**	**0.275**	**0.348**	**0.508**	**0.722**
1.5	**-0.236**	**-0.107**	**0.028**	**0.095**	**0.163**	**0.231**	**0.302**	**0.464**	**0.696**
2	**-0.240**	**-0.122**	**0.005**	**0.070**	**0.136**	**0.205**	**0.277**	**0.447**	**0.688**
40	**-0.244**	**-0.125**	**0.0001**	**0.065**	**0.133**	**0.204**	**0.267**	**0.440**	**0.684**

Table 2 Normalized T_{33} solutions (β_{33}) at the specimen mid-plane for 3PB specimens (ν= 0.3)

a/W									
B/W	**0.2**	**0.3**	**0.4**	**0.45**	**0.5**	**0.55**	**0.6**	**0.7**	**0.8**
0.1	**-0.861**	**-1.041**	**-1.184**	**-1.245**	**-1.301**	**-1.351**	**-1.395**	**-1.461**	**-1.458**
0.25	**-0.530**	**-0.617**	**-0.682**	**-0.708**	**-0.728**	**-0.742**	**-0.749**	**-0.725**	**-0.587**
0.5	**-0.353**	**-0.388**	**-0.404**	**-0.405**	**-0.399**	**-0.386**	**-0.362**	**-0.262**	**-0.041**
1	**-0.246**	**-0.206**	**-0.168**	**-0.144**	**-0.115**	**-0.079**	**-0.036**	**0.073**	**0.205**
1.5	**-0.216**	**-0.142**	**-0.072**	**-0.038**	**-0.003**	**0.033**	**0.070**	**0.147**	**0.230**
2	**-0.197**	**-0.118**	**-0.040**	**-0.004**	**0.031**	**0.065**	**0.097**	**0.159**	**0.232**
40	**-0.059**	**-0.024**	**0.011**	**0.030**	**0.049**	**0.069**	**0.114**	**0.166**	**0.236**

Table A.1 Summary of the generated mesh (W = 25 mm, S/W = 4, R_s = 0.4 mm)

B/*W*	*a*/*W*	0.2	0.3	0.4	0.45	0.5	0.55	0.6	0.7	0.8
0.1	Δ*l*/*a*	4.0	2.7	2.0	1.8	1.6	1.5	1.3	1.1	1.0
	CD	12	16	20	26	30	34	40	48	56
	NR	61	53	45	41	37	33	29	21	13
	na (na_bias)	189 (2)								
0.25	Δ*l*/*a*	4.0	2.7	2.0	1.8	1.6	1.5	1.3	1.1	1.0
	CD	12	16	20	26	30	34	40	48	56
	NR	61	53	45	41	37	33	29	21	13
	na (na_bias)	189 (2)								
0.5	Δ*l*/*a*	4.0	2.7	2.0	1.8	1.6	1.5	1.3	1.1	1.0
	CD	12	16	20	26	30	34	40	48	56
	NR	61	53	45	41	37	33	29	21	13
	na (na_bias)	189 (2)								
1	Δ*l*/*a*	4.0	2.7	2.0	1.8	1.6	1.5	1.3	1.1	1.0
	CD	12	16	20	26	30	34	40	48	56
	NR	61	53	45	41	37	33	29	21	13
	na (na_bias)	189 (2)								

	NR	**61**	**53**	**45**	**41**	**37**	**33**	**29**	**21**	**13**
	na (na_bias)	**189 (2)**								
1.5	***Na***	**4.0**	**2.7**	**2.0**	**1.8**	**1.6**	**1.5**	**1.3**	**1.1**	**1.0**
	CD	**12**	**16**	**20**	**26**	**30**	**34**	**40**	**48**	**56**
	NR	**61**	**53**	**45**	**41**	**37**	**33**	**29**	**21**	**13**
	na (na_bias)	**189 (2)**								
2	***Na***	**4.0**	**2.7**	**2.0**	**1.8**	**1.6**	**1.5**	**1.3**	**1.1**	**1.0**
	CD	**12**	**16**	**20**	**26**	**30**	**34**	**40**	**48**	**56**
	NR	**61**	**53**	**45**	**41**	**37**	**33**	**29**	**21**	**13**
	na (na_bias)	**189 (2)**								
40	***Na***	**4.0**	**2.7**	**2.0**	**1.8**	**1.6**	**1.5**	**1.3**	**1.1**	**1.0**
	CD	**12**	**15**	**24**	**20**	**20**	**24**	**30**	**40**	**45**
	NR	**50**	**50**	**36**	**36**	**36**	**32**	**28**	**20**	**12**
	na (na_bias)	**18 9 (2)**	**24 3(1)**							

Highlights

- T-stress solutions 3PB specimens with various crack depths and thicknesses were obtained.
- Mid-plane T_{11} and T_{33} were reported for 3PB specimens with a/W =0.2~0.8 and B/W =0.1 ~ 40.
- T_{11} showed 3D effect, and approached 2D plane strain solutions for large thickness.
- T_{33} increased with thickness, and saturated to vT_1 for $B/W \geq 2$.

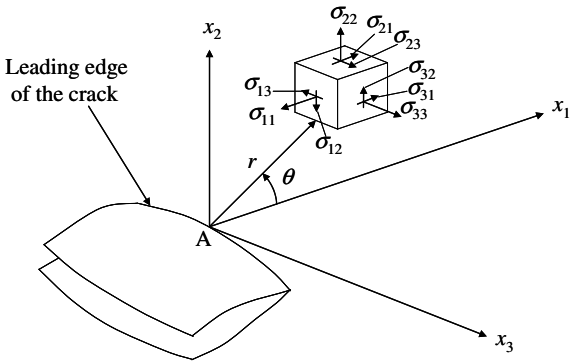

Fig. 1 Three-dimensional coordinate system for the region along the crack front

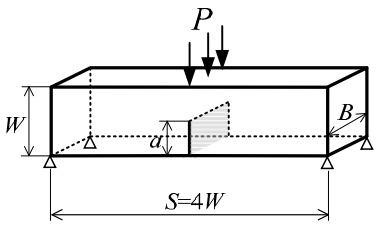

Fig. 2 Sketch of the loads and geometry of the 3PB specimens

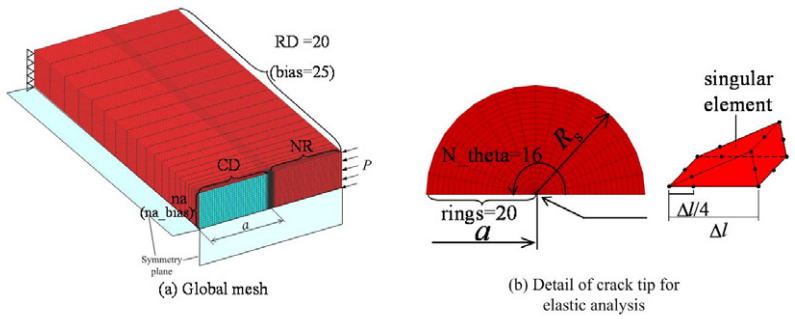

Fig. 3 Typical finite element model of a 3PB specimen
(W = 25 mm, S/W = 4, a/W = 0.5, B/W = 0.5)

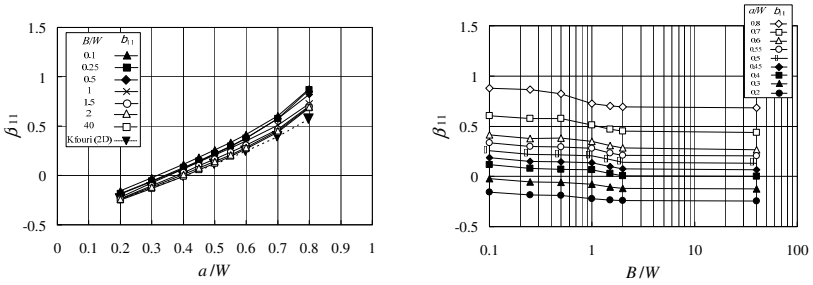

(a) b_{11} vs a/W (b) b_{11} vs B/W

Fig. 4 Normalized T_{11} solutions (β_{11}) at the specimen mid-plane for 3PB specimens ($\nu = 0.3$)

4

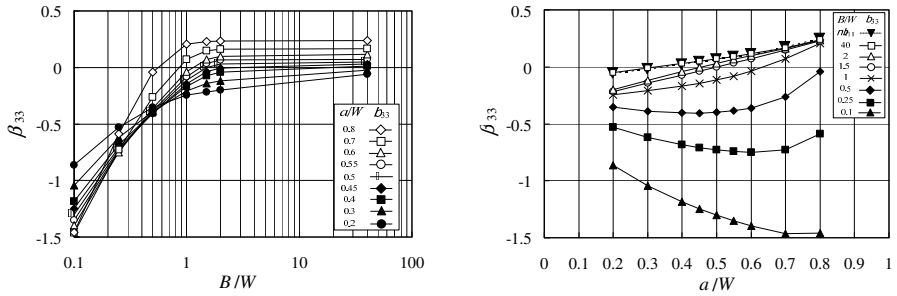

(a) b_{33} vs B/W (b) b_{33} vs a/W

Fig. 5 Normalized T_{33} solutions (β_{33}) at the specimen mid-plane for 3PB specimens ($\nu = 0.3$)

5

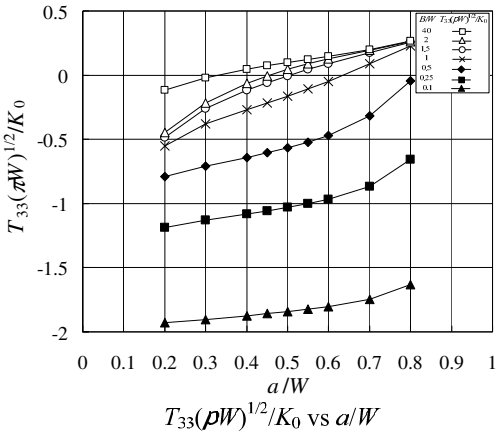

Fig. 6 Normalized T_{33} solutions ($T_{33}(\pi W)^{1/2}/K_0$) at the specimen mid-plane for 3PB specimens ($\nu = 0.3$)

6

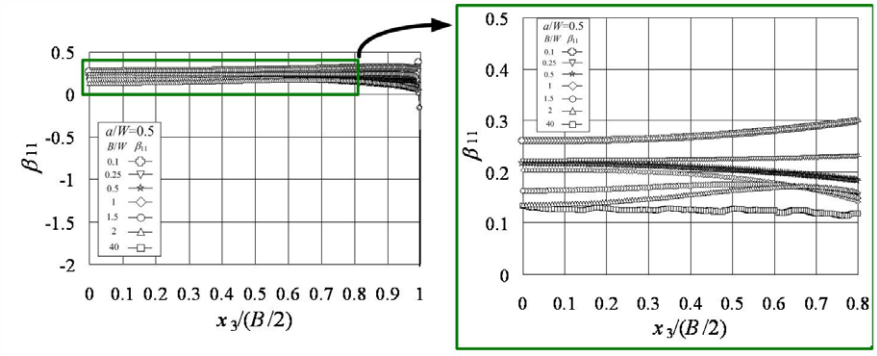

Fig. 7 Variations of β_{11} in the thickness direction along the crack front for various thicknesses when $a/W = 0.5$ ($\nu = 0.3$)

7

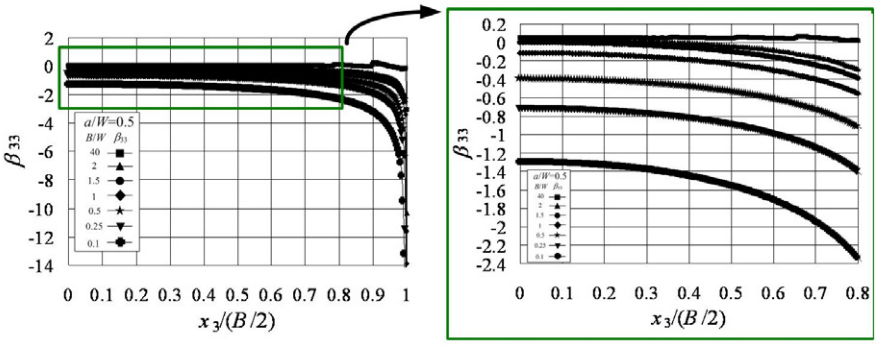

Fig. 8 Variations of β_{33} in the thickness direction along the crack front for various thicknesses when $a/W = 0.5$ ($\nu = 0.3$)